

# OnlinePG: Online Open-Vocabulary Panoptic Mapping with 3D Gaussian Splatting

Hongjia Zhai<sup>1,2</sup> Qi Zhang<sup>2</sup> Xiaokun Pan<sup>1</sup> Xiyu Zhang<sup>1</sup> Yitong Dong<sup>1,2</sup>  
 Huaqi Zhang<sup>2</sup> Dan Xu<sup>3</sup> Guofeng Zhang<sup>1†</sup>

<sup>1</sup>State Key Lab of CAD & CG, Zhejiang University <sup>2</sup>VIVO BlueImage Lab <sup>3</sup>HKUST

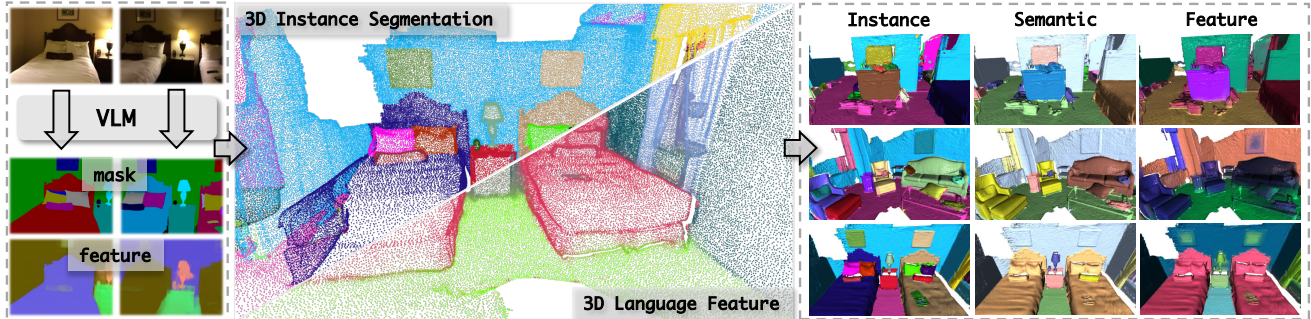


Figure 1. **Illustration of OnlinePG**, which integrates geometric reconstruction and open-vocabulary panoptic perception built upon 3D Gaussian Splatting. Given the posed video stream and 2D noise priors (mask and feature) generated by vision-language models (VLMs), OnlinePG can reconstruct a consistent 3D language feature field and perform online open-vocabulary panoptic mapping.

## Abstract

*Open-vocabulary scene understanding with online panoptic mapping is essential for embodied applications to perceive and interact with environments. However, existing methods are predominantly offline or lack instance-level understanding, limiting their applicability to real-world robotic tasks. In this paper, we propose OnlinePG, a novel and effective system that integrates geometric reconstruction and open-vocabulary perception using 3D Gaussian Splatting in an online setting. Technically, to achieve online panoptic mapping, we employ an efficient local-to-global paradigm with a sliding window. To build local consistency map, we construct a 3D segment clustering graph that jointly leverages geometric and semantic cues, fusing inconsistent segments within sliding window into complete instances. Subsequently, to update the global map, we construct explicit grids with spatial attributes for the local 3D Gaussian map and fuse them into the global map via robust bidirectional bipartite 3D Gaussian instance matching. Finally, we utilize the fused VLM features inside the 3D spatial attribute grids to achieve open-vocabulary scene understanding. Extensive experiments on widely used datasets demonstrate that our method achieves better performance among online approaches, while maintaining real-time efficiency.*

<sup>†</sup>Corresponding author.

## 1. Introduction

Open-vocabulary 3D scene understanding is fundamental for embodied tasks, enabling robots to perceive, reason about, and interact with complex environments using natural language and instruction [9, 31, 33, 38]. While significant progress has been made in offline settings, real-world robotic applications demand online perception and mapping capabilities [23, 27, 61] that can process streaming data and support decision-making in real time.

To overcome the limited capability of annotated 3D data, recent works [16, 22, 28, 48, 49] leverage various 2D vision-language models (VLMs) [1, 10, 17, 29, 34, 35] to transfer open-vocabulary knowledge into 3D space. Building on differentiable rendering techniques such as Neural Radiance Fields (NeRF) [26] and 3D Gaussian Splatting (3DGS) [11], several methods [6, 19, 33, 38, 50, 58] have achieved impressive results in fine-grained open-vocabulary scene understanding. However, these approaches are predominantly offline and lack support for online instance-level panoptic perception, hindering their applications in embodied tasks.

Despite previous approaches that combine VLMs with 3DGS having yielded satisfactory performance, two critical limitations remain: 1) *offline reconstruction and perception settings*. Most existing reconstruction and understanding methods [33, 38, 50, 58] require pre-collected data. This offline setting prevents robots from simultaneously exploring and understanding unknown environments in real

time. Online mapping and perception are indispensable for robots. 2) *missing or inaccurate 3D instance-level understanding*. Current online open-vocabulary scene understanding approaches [42, 52] cannot distinguish individual 3D instances based on text queries, while offline instance-aware approaches [19, 39, 50, 58] rely on time-consuming clustering or multi-view guidance that is unsuitable for online systems. However, equipping the online mapping system with capabilities of open-vocabulary panoptic understanding is highly meaningful and needed for embodied applications. Addressing these challenges is crucial for enabling real-time, open-vocabulary panoptic mapping and understanding in embodied applications.

To this end, we present OnlinePG, an efficient online open-vocabulary panoptic mapping system based on 3D Gaussian Splatting that integrates geometric reconstruction with semantic understanding. Our key insight is to employ an efficient local-to-global paradigm: we first build local consistent maps within a sliding window to mitigate noisy 2D VLM priors, then incrementally fuse them into a global representation. Specifically, given noisy 2D masks and feature maps from VLMs, we initialize 3D Gaussian segments from keyframes and construct a multi-cue clustering graph that leverages geometric overlap, semantic similarity, and view consensus to merge inconsistent segments into complete instances. We then voxelize the local map to build explicit spatial attribute grids for storing semantic features and instance labels, which are robustly fused into the global map via our bidirectional bipartite matching scheme. This design enables accurate instance-level open-vocabulary understanding while maintaining real-time performance.

Overall, the technical contributions of our approach are summarized as follows:

- We propose an online open-vocabulary panoptic mapping framework that unifies geometric reconstruction and semantic understanding in a local-to-global paradigm.
- We develop a multi-cue segment clustering algorithm that synergistically leverages geometric, semantic, and view consensus information to obtain local consistent 3D instances from noisy 2D VLM priors.
- We design a bidirectional bipartite matching scheme with explicit spatial attributes for robust incremental fusion of local 3D instances into the global map.
- Extensive experiments demonstrating our superior performance among online methods, with significant improvements in both semantic and panoptic metrics.

## 2. Related Work

**Panoptic Segmentation.** 2D panoptic segmentation task was first proposed by Kirillov *et al.* [13], which aims to understand objects with different semantics and instances within images. Follow-up works [3, 4, 32] have attempted to advance the CNN model’s ability to reason and under-

stand images from a human perspective. To explore spatial semantics and understand 3D scenes, some works [7, 16, 28, 39, 58, 64] integrate and lift 2D panoptic predictions of 2D models [4, 21] into 3D space. Inspired by [25], PanopticFusion [28] fuses the 2D panoptic information into 3D volume and performs map regularization. In addition, some works [16, 19, 58] have exploited recent optimization and rendering capabilities of differentiable representations [11, 26] to understand 3D scenes. However, limited by the offline or closed-set setting, these works cannot simultaneously perform online 3D panoptic reconstruction or open vocabulary 3D scene understanding.

**Online 3D Scene Mapping and Perception.** For real-world applications of embodied intelligence [9, 27, 56, 61], intelligent robots typically perceive and understand the environment with an online data stream. Previous online 3D scene mapping and perception methods [22, 28, 36, 41, 51, 52] were generally implemented by projecting 2D semantic predictions back into 3D scene maps. Accurately reconstructing and understanding the surrounding 3D scene from RGB-D video streams is the visual foundation for these robotic tasks. Benefiting from NeRF/3DGS-based reconstruction [18, 59, 60, 62], recent works [30, 42, 45, 54, 56, 57, 65] have incorporated NeRF and 3DGS for fine-grained, better online mapping and perception performance. However, these online approaches cannot achieve instance-aware panoptic mapping and perception for open-vocabulary scene understanding.

**Open Vocabulary 3D Scene Understanding.** 3D scene understanding plays an important role in embodied intelligence. However, limited 3D annotated datasets [5, 40] have hindered the development of open-vocabulary 3D scene understanding, with most works [37, 44, 51] only achieving good results in closed-vocabulary settings. With the rapid advancement of 2D VLM [1, 17, 34], some efforts [31, 58] use 3D consistent feature fields to model the scene property with the lifted 2D VLM features as supervision information. LERF [12] and N3F [43] are the first batch of works that combine NeRF and VLMs for open vocabulary 3D scene understanding, learning consistent feature fields in 3D space through volume rendering. And the follow-up works [2, 8, 38, 63, 66] replace NeRF with 3DGS for efficient rendering and explicit 3D scene representation. Besides, to distinguish the instance information of 3D Gaussian primitives, the recent PanoGS [58] and InstanceGaussian [19] use 2D instance information of SAM [14] to guide the 3D Gaussian clustering. Those offline approaches adopt contrastive feature learning [8, 50, 55] to group 3D Gaussian primitives into complete instances. Due to the inherently slow convergence of this mechanism, adapting it to online mapping systems will result in inaccurate 3D instance results. Therefore, their offline setting hinders scene understanding applications for online embodied tasks.

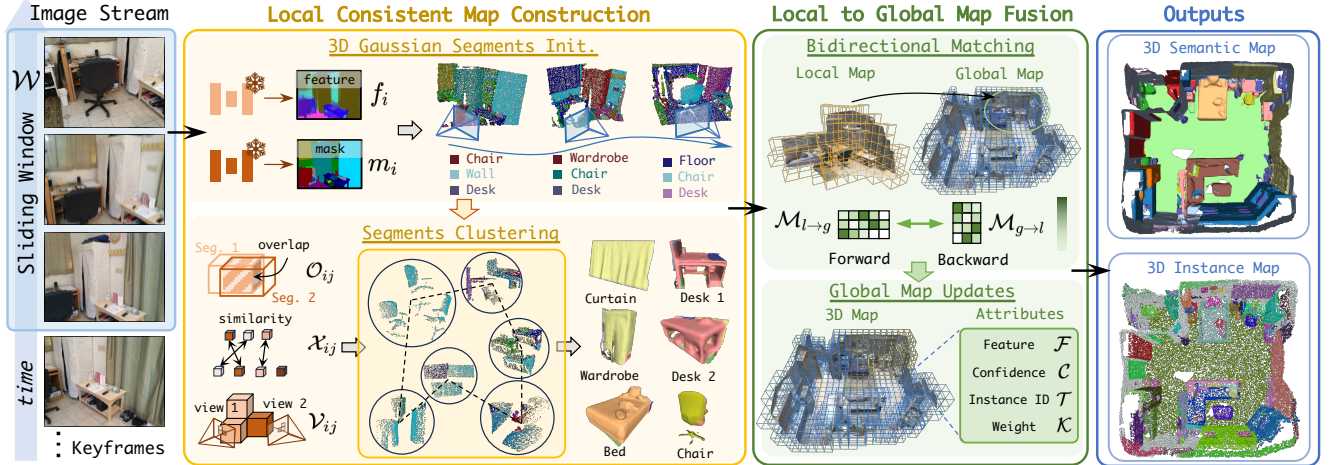


Figure 2. **Overview of Our Approach.** Our system performs online open-vocabulary panoptic mapping from RGB-D streams using a local-to-global paradigm. (a) Maintaining a sliding window  $\mathcal{W}$  to build locally consistent instance and fuse them globally. (b) Using noisy 2D masks and features from [17, 21] to initialize 3D Gaussian segments, which are clustered via multi-cues to form consistent 3D instances. (c) Bidirectional bipartite matching incrementally fuses local instances and spatial attributes into the global map.

### 3. Method

As shown in Fig. 2, given the posed RGB-D stream, we can perform 3D online open-vocabulary panoptic mapping, which formulates the pipeline as an efficient local-to-global paradigm. To mitigate the inconsistencies of 2D segmentation results, we propose an effective segment clustering algorithm that synergistically leverages geometric and semantic cues to obtain consistent 3D Gaussian instances. Then we construct a grid-based spatial attribute that stores semantic information of the reconstructed scene (Sec. 3.2). Finally, we design a bidirectional bipartite matching scheme to incrementally fuse local 3D Gaussian instances and spatial attribute grids into global map (Sec. 3.3).

#### 3.1. Scene Representation

**3D Gaussian Splatting.** Benefiting from the efficiency of 3DGS [11], we represent the 3D scene with 3D Gaussians for online open vocabulary panoptic mapping. We incrementally reconstruct the 3D Gaussian primitives from the RGB-D stream:

$$\mathcal{G}_i := \{\mu_i, \Sigma_i, \sigma_i, \mathbf{c}_i\}, \quad (1)$$

where each Gaussian primitive  $\mathcal{G}_i$  contains its position  $\mu_i \in \mathbb{R}^3$ , covariance matrix  $\Sigma_i \in \mathbb{R}^{3 \times 3}$ , opacity  $\sigma_i \in \mathbb{R}$ , and color  $\mathbf{c}_i \in \mathbb{R}^3$ .

The 3D scene properties can be rasterized to the 2D image plane via fast differentiable rasterization [24] for differentiable optimization. Following previous works [11, 23], we adopt the L1 loss terms for appearance and geometry optimization:

$$\mathcal{L} = \alpha \cdot \mathcal{L}_c + (1 - \alpha) \cdot \mathcal{L}_d, \quad (2)$$

where  $\alpha$  is the weight for the optimization components.

**Grid-based Spatial Attributes.** In addition to these anisotropic attributes bound to Gaussian primitives, we require additional representations to model open-vocabulary panoptic information. Therefore, for efficient computation and lightweight storage, we perform voxelization on the reconstructed regions and adopt explicit sparse grids to record spatial geometric and semantic attributes. The spatial attributes are represented by a set of sparse voxel grids, where each occupied voxel contains  $\{\mathcal{F}, \mathcal{C}, \mathcal{T}, \mathcal{K}\}$ :  $\mathcal{F} \in \mathbb{R}^{D_f}$  stores language features extracted from VLMs,  $\mathcal{C} \in \mathbb{R}$  is the confidence of the feature,  $\mathcal{T} \in \mathbb{R}$  is the panoptic instance label, and  $\mathcal{K} \in \mathbb{R}$  is the instance weight. These grids are detailed in the following sections.

#### 3.2. Local Consistent Map Construction

To obtain accurate 3D Gaussian instances, existing methods adopt contrastive feature learning [19, 50, 55] guided by inconsistent 2D masks. However, this paradigm is unsuitable for online reconstruction due to slow convergence and time-consuming post-processing. Since 2D segmentation priors are inherently noisy (e.g., multi-view inconsistency, over-segmentation), directly lifting and fusing 2D keyframes into the 3D map [25, 28] is both inaccurate and inefficient. Therefore, we maintain a sliding window over the input stream and perform 3D segment clustering to obtain consistent instances while mitigating noise from 2D priors.

**3D Gaussian Segments Initialization.** For  $i$ -th keyframe inside the sliding window  $\mathcal{W}$ , we use LSeg [17] and EntitySeg [21] to extract its 2D feature map  $f_i \in \mathbb{R}^{H \times W \times D_f}$  and instance mask  $m_i \in \mathbb{R}^{H \times W}$ . We then lift the keyframe

into 3D space using its depth value to initialize 3D Gaussian primitives. The Gaussian primitives are grouped into multiple 3D segments according to their corresponding 2D mask IDs: primitives sharing the same mask ID in  $m_i$  are assigned to the same segment. For simplicity, we refer to a group of Gaussian primitives with the same instance ID as a 3D segment  $\mathcal{S}_i$ . In this way, we obtain multiple 3D segments initialized from keyframes inside the sliding window.

$$\mathcal{S} := \{\mathcal{S}_1, \dots, \mathcal{S}_n, |\mathcal{S}_i := \{\mathcal{G}_j\}_{j=1}^n}\}, \quad (3)$$

where  $|m_i|$  is the 2D instance number of  $I_i$ , and  $n = \sum_{i \in \mathcal{W}} |m_i|$  is the 3D segment number inside the window.

Due to the inconsistency of 2D segmentation  $m_i$ , the resulting 3D segments  $\mathcal{S}$  may be over-segmented or under-segmented. To obtain consistent instances from  $\mathcal{W}$  for subsequent reconstruction and rendering, we construct a clustering graph for the inconsistent  $\mathcal{S}$  and cluster them based on their mutual relationships to obtain the consistent 3D Gaussian instances  $\mathcal{I}$ .

**Segments Clustering Graph with Multi-cues.** We formulate the clustering graph as  $(\{\mathcal{S}_i\}, \{\mathcal{E}_{ij}\})$ , where 3D segments are defined as the vertices  $\mathcal{S}_i$ , and the edges  $\mathcal{E}_{ij}$  represent the affinity between different segments, reflecting the probability that segments belong to the same instance. To capture the detailed affinity, we take the geometry, semantic, and view consensus cues into consideration.

**(1) Geometry cue:** Since each 3D segment contains multiple 3D Gaussian primitives with varying densities, traversing all primitives for overlap computation is time-consuming. To efficiently calculate the overlap between different Gaussian segments, we uniformly divide the space into axis-aligned voxels of specified size and count the overlapped voxels instead:

$$\mathcal{O}(\mathcal{S}_i, \mathcal{S}_j) = \frac{1}{2} \cdot \left( \frac{|\mathcal{S}_i \cap \mathcal{S}_j|}{\text{Cont.}(\mathcal{S}_i, \mathcal{S}_j)} + \frac{|\mathcal{S}_i \cap \mathcal{S}_j|}{\text{Cont.}(\mathcal{S}_j, \mathcal{S}_i)} \right), \quad (4)$$

where  $\text{Cont.}(\mathcal{S}_i, \mathcal{S}_j)$  denotes the ratio of visible voxels in  $\mathcal{S}_j$  that are contained in  $\mathcal{S}_i$  when projecting  $\mathcal{S}_j$  back to the viewpoint of  $\mathcal{S}_i$ .

**(2) Semantic cue:** To obtain the language feature for segment  $\mathcal{S}_i$ , we pool the language feature map according to its 2D mask:  $z_i = \Phi(\{f(u, v) : m(u, v) = i\})$ , where  $\Phi(\cdot)$  denotes average pooling. The semantic cue is then computed as the cosine similarity between language features:  $\mathcal{X}(\mathcal{S}_i, \mathcal{S}_j) = z_i \cdot z_j / (\|z_i\| \cdot \|z_j\|)$ .

**(3) View consensus cue:** We use the view consensus rate from [53] as additional criteria to judge whether two segments belong to the same 3D instance.

$$\mathcal{V}(\mathcal{S}_i, \mathcal{S}_j) = \frac{N_{\text{supp}}(\mathcal{S}_i, \mathcal{S}_j)}{N_{\text{vis}}(\mathcal{S}_i, \mathcal{S}_j)}, \quad (5)$$

where  $N_{\text{supp}}$  and  $N_{\text{vis}}$  represent the number of keyframes where both segments are contained and visible.

**Clustering for Local Consistent Map.** Once the clustering graph  $(\{\mathcal{S}_i\}, \{\mathcal{E}_{ij}\})$  is constructed, we perform graph-based clustering to merge over-segmented and under-segmented results from the sliding window into consistent 3D instances. To determine whether two segments should be merged, we adopt the following criteria:

$$\Delta_{ij} = ((\mathcal{O}_{ij} + \mathcal{X}_{ij}) > \lambda_1) \cup (\mathcal{V}_{ij} > \lambda_2), \quad (6)$$

where  $\lambda_1$  and  $\lambda_2$  are the threshold parameters controlling the merging decision.

We iterate through the graph using Eq. (6) to identify connected components, with each component representing a consistent instance. The final consistent 3D Gaussian instances  $\mathcal{I}$  are obtained via:

$$\mathcal{I} = \text{Cluster}(\{\mathcal{S}_i\}, \{\mathcal{E}_{ij} := \{\mathcal{O}_{ij}, \mathcal{X}_{ij}, \mathcal{V}_{ij}\}\}), \quad (7)$$

where  $\text{Cluster}(\cdot)$  denotes the clustering operation based on connected components.

Through this multi-cue graph clustering algorithm, we obtain geometrically and semantically consistent 3D Gaussian instances  $\mathcal{I}$  from the local sliding window.

**Local Spatial Attribute Grids.** After clustering the 3D Gaussian segments, we voxelize the 3D space to efficiently compute and update spatial attributes. For each voxel  $v$  occupied by instance  $\mathcal{I}_i$ , we assign the local instance label and weight grids:

$$\mathcal{T}_l^t(v) = \text{ID}_i, \quad \mathcal{K}_l^t(v) = N_i, \quad (8)$$

where  $t$  denotes the time index,  $l$  denotes the local map,  $\text{ID}_i$  is the instance ID of  $\mathcal{I}_i$ , and  $N_i$  is the number of observations of  $\mathcal{I}_i$  during clustering, reflecting its confidence and frequency.

To enable open-vocabulary scene understanding, we aggregate multi-view language features from the sliding window  $\mathcal{W}$  into local feature grid  $\mathcal{F}_l^t$  and confidence grid  $\mathcal{C}_l^t$ :

$$\mathcal{F}_l^t(v) = \frac{1}{\mathcal{C}_l^t(v)} \sum_{i \in \mathcal{W}} c_i(u, v) \cdot f_i(u, v), \quad (9)$$

where  $\mathcal{C}_l^t(v) = \sum_{i \in \mathcal{W}} c_i(u, v)$  and  $c_i$  is the confidence map of feature  $f_i$ .

### 3.3. Local-to-Global Map Fusion

After reconstructing the local 3D Gaussian instance map and spatial attribute grids from the sliding window  $\mathcal{W}$ , we match and register them into the global map. To establish accurate matches between local and global maps, we leverage geometric and semantic information from the spatial attribute grids to construct correspondence score matrix.

**Bidirectional Bipartite Matching.** To establish one-to-one correspondences between local and global maps, we first

construct a forward correspondence score matrix  $\mathcal{M}_{l \rightarrow g} \in \mathbb{R}^{n_l \times n_g}$ :

$$\mathcal{M}_{l \rightarrow g} = \frac{z_l \cdot z_g}{\|z_l\| \cdot \|z_g\|} + \frac{|\mathcal{I}_l \cap \mathcal{I}_g|}{\text{Cont.}(\mathcal{I}_l, \mathcal{I}_g)}, \quad (10)$$

where  $n_l$  and  $n_g$  are the numbers of instances in the local and global maps, and  $z_l$  is the instance-level language feature of  $\mathcal{I}_l$  queried from feature grid  $\mathcal{F}_l$ .

However, since the local map contains newly explored regions while the global map contains historical regions, the correspondence matrix is inherently asymmetric, particularly in geometric containment ratios. To achieve robust matching, we construct a backward correspondence matrix  $\mathcal{M}_{g \rightarrow l} \in \mathbb{R}^{n_g \times n_l}$  by replacing the second term in Eq. (10) with  $(|\mathcal{I}_g \cap \mathcal{I}_l|)/\text{Cont.}(\mathcal{I}_g, \mathcal{I}_l)$ .

With the above bidirectional matching matrix  $\mathcal{M}_{l \rightarrow g}$  and  $\mathcal{M}_{g \rightarrow l}$ , we perform forward and backward bipartite graph matching via the Hungarian algorithm [15] to yield the robust matching results:

$$\mathcal{A} = \text{Hung.}(\mathcal{M}_{l \rightarrow g}) \cap \text{Hung.}(\mathcal{M}_{g \rightarrow l})^T, \quad (11)$$

where  $\mathcal{A}$  is the final set of matched correspondences,  $\text{Hung.}(\cdot)$  is the Hungarian algorithm, and  $(\cdot)^T$  denotes transpose to ensure bidirectional consistency. This bidirectional strategy ensures reliable matching by requiring mutual agreement between forward and backward directions.

**Global Map Update.** For each voxel  $v$  occupied by a clustered instance  $\mathcal{I}$ , we update the global feature grid  $\mathcal{F}_g^t$  and confidence grid  $\mathcal{C}_g^t$  using weighted averaging:

$$\mathcal{F}_g^t(v) = \frac{\mathcal{C}_l^t(v) \cdot \mathcal{F}_l^t(v) + \mathcal{C}_g^{t-1}(v) \cdot \mathcal{F}_g^{t-1}(v)}{\mathcal{C}_g^t(v)}, \quad (12)$$

where  $\mathcal{C}_g^t(v) = \mathcal{C}_l^t(v) + \mathcal{C}_g^{t-1}(v)$  is the updated confidence.

Since spatial attributes store discrete instance information in voxel form, we cannot perform continuous gradient updates. Instead, we update the instance label  $\mathcal{T}_g^t$  and weight  $\mathcal{K}_g^t$  grids similar to [25, 28]:

- **For matched instances:** We merge the matched instances into the global map by increasing the weight for each occupied voxel  $v$ :

$$\mathcal{T}_g^t(v) = \mathcal{T}_g^{t-1}(v), \quad \mathcal{K}_g^t(v) = \mathcal{K}_g^{t-1}(v) + \mathcal{K}_l^t(v). \quad (13)$$

- **For unmatched instances:** If  $\mathcal{K}_l^t(v) \leq \mathcal{K}_g^{t-1}(v)$ , we retain the global instance but decrease its weight:

$$\mathcal{T}_g^t(v) = \mathcal{T}_g^{t-1}(v), \quad \mathcal{K}_g^t(v) = \mathcal{K}_g^{t-1}(v) - \mathcal{K}_l^t(v). \quad (14)$$

If  $\mathcal{K}_l^t(v) > \mathcal{K}_g^{t-1}(v)$ , indicating the local segmentation is more reliable, we replace the global instance:

$$\mathcal{T}_g^t(v) = \mathcal{T}_l^t(v), \quad \mathcal{K}_g^t(v) = \mathcal{K}_l^t(v) - \mathcal{K}_g^{t-1}(v). \quad (15)$$

Through our bidirectional bipartite matching and robust fusion strategy, we can effectively integrate local 3D Gaussian instances and spatial attributes into the global map, enabling accurate and consistent online open-vocabulary panoptic mapping.

## 4. Experiments

In this section, we introduce our experimental settings and present open-vocabulary panoptic mapping results on two commonly used datasets. Additionally, we perform a detailed ablation study to validate the effect of each design in our system.

### 4.1. Experimental Settings

**Datasets.** Following the previous works [31, 42, 50, 58], we evaluate the quantitative and qualitative performance on a variety of scenes from two commonly used datasets, ScanNetV2 [5] and Replica [40]. The two datasets both contain high-quality RGB-D sequences of various indoor scenes and 3D instance-level semantic annotations. Following [50, 58], we take the commonly-used 8 scenes {room0-2, office0-4} for Replica dataset. For the ScanNetV2 dataset, we use the same 10 selected sequences and settings for evaluation.

**Evaluation Metrics.** For open-vocabulary panoptic mapping evaluation, we adopt four widely-used metrics: 3D point-level mean Intersection over Union (mIoU), mean Accuracy (mAcc), and 3D Panoptic Reconstruction Quality at *thing*-level (PRQ (T)) and *stuff*-level (PRQ (S)). Unlike offline baselines [33, 50, 58] that use ground truth point clouds as input, our method reconstructs the scene from RGB-D streams. Therefore, we project our reconstructed results to the ground truth point clouds for evaluation.

**Implementation Details.** Following [31, 58], we adopt CLIP [34] and LSeg [17] as text and image visual-language feature extractors, with feature dimension  $D_f = 512$ . We use EntitySeg [21] to extract 2D instance segmentation for each keyframe. The hyperparameters are set as:  $\alpha = 0.9$ ,  $\lambda_1 = 1.5$ ,  $\lambda_2 = 0.8$ . We sample a keyframe every 20 frames and maintain a sliding window of size 12. Segment clustering and local-to-global map fusion are performed every 7 keyframes. The voxel size for spatial attributes is 3 cm. For 3D Gaussian rendering optimization, when adding a new keyframe, we randomly select 5 historical keyframes and perform 20 optimization iterations using Eq. (2).

**Baselines.** To compare our approach with recent open-vocabulary methods, we take five offline approaches: LangSplat [33], OpenGaussians [50], OpenScene [31], InstanceGaussian [19], PanoGS [58], and two recent online approaches: O2V-Mapping [42], OnlineAnySeg [41] as baselines. Since the baselines [31, 33, 50] marked with \* cannot obtain 3D panoptic results, we use the performance reported in [58], which uses a supervised 3D instance seg-

Table 1. **3D Semantic and Panoptic Segmentation Results on ScanNetV2 and Replica Datasets.** \* indicates the baseline results are taken from [58] which use the 3D instance obtained from supervised approach [44] for panoptic comparison (their panoptic results are marked in gray). We mark the top-3 segmentation results among all approaches in **red**, **green**, and **blue**, respectively.

Methods	Online	Pano.	ScanNetV2 [5]				Replica [40]			
			mIoU $\uparrow$	mAcc. $\uparrow$	PRQ (T) $\uparrow$	PRQ (S) $\uparrow$	mIoU $\uparrow$	mAcc. $\uparrow$	PRQ (T) $\uparrow$	PRQ (S) $\uparrow$
LangSplat [33]*	$\times$	$\times$	29.47	45.29	22.57	28.44	4.82	10.03	8.29	1.28
OpenGaussian [50]*	$\times$	$\times$	24.89	37.35	22.87	19.71	–	–	–	–
OpenScene [31]*	$\times$	$\times$	47.63	69.74	43.53	40.43	49.03	62.89	33.04	11.84
InstanceGaussian [19]	$\times$	$\checkmark$	34.14	54.95	<b>39.04</b>	27.41	–	–	–	–
PanoGS [58]	$\times$	$\checkmark$	<b>50.72</b>	<b>70.20</b>	33.84	36.22	<b>54.98</b>	<b>67.35</b>	<b>43.04</b>	<b>30.60</b>
O2V-Mapping [42]	$\checkmark$	$\times$	33.74	55.52	–	–	24.35	33.62	–	–
OnlineAnySeg [41]	$\checkmark$	$\checkmark$	31.28	52.20	35.98	26.27	37.48	45.64	34.19	9.13
Ours	$\checkmark$	$\checkmark$	48.48	66.01	37.97	41.81	47.93	54.94	41.02	12.83



Figure 3. **Qualitative 3D Semantic Segmentation Comparison of ScanNetV2 Dataset.** Our approach outperforms recent online approaches, O2V-Mapping [42] and OnlineAnySeg [41], by a large margin. Compared with the offline SOTA PanoGS [58], our approach still exists a small performance gap.

mentation approach [44] (trained on ScanNetV2 [5]) to obtain 3D instances for them. So, we mark their PRQ performance in gray.

## 4.2. Main Experiments

We evaluate the 3D panoptic segmentation metrics of our approach and baseline on two commonly used ScanNetV2 [5] and Replica [40] datasets. The averaged quantitative 3D semantic and panoptic segmentation results are

shown in Tab. 1. We mark the top-3 segmentation results among all approaches in **red**, **green**, and **blue**, respectively.

**3D Semantic Segmentation.** As shown in Tab. 1, our method achieves the best 3D semantic segmentation results among online approaches on the mIoU and mAcc metrics of two datasets. Compared to O2V-Mapping [42] and OnlineAnySeg [41], by maintaining and updating voxel-level spatial language feature grid  $\mathcal{F}$ , we can achieve more fine-grained 3D scene understanding performance, thereby

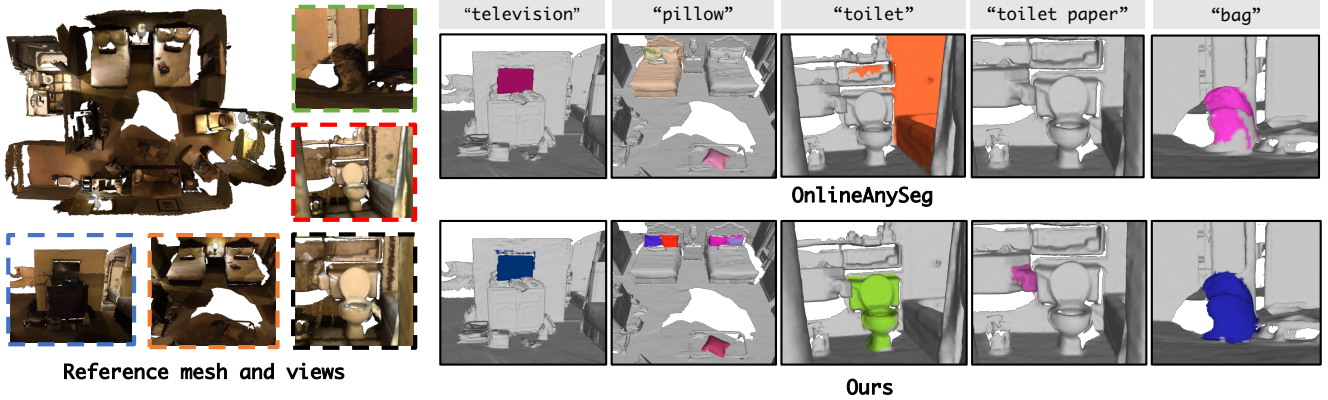


Figure 4. **Qualitative Results of Open-Vocabulary Query.** We use different colors to distinguish different instances found in the query. Compared to OnlineAnySeg [41], our approach shows advanced text query capabilities for long-tail and multiple instances scenario.

avoiding language feature drift caused by fusing features from the noise instance parts. Compared to the best current offline method, OnlineAnySeg [41], we outperformed by  $\sim 13.8$  and  $\sim 11.5$  in mIoU and mAcc. metrics, respectively. While a performance gap remains compared to offline methods [31, 58] that use ground truth point clouds and capture global multi-view information, our method substantially narrows this gap. Besides, we show some qualitative open-vocabulary 3D semantic segmentation results of ScanNetV2 in Fig. 3. As shown in the figure, previous online methods only maintained instance-level language features, which led to inaccurate semantic segmentation of open vocabularies due to inaccurate instances and language feature drifts during blending. Our method can achieve more consistent segmentation results among online approaches.

**3D Panoptic Segmentation.** Since some offline baselines (LangSplat [33], OpenGaussian [50], OpenScene [31]) marked with \* cannot inherently output 3D instances, PanoGS [58] provides supervised instance annotations [44] for them to compute PRQ metrics (marked in gray). As shown in Tab. 1, compared to the performance gap in 3D semantic segmentation, we further narrow the gap with offline baselines in 3D panoptic segmentation performance, even surpassing PanoGS [58] on the ScanNetV2 [5] dataset. The performance also validates the effectiveness of our local-to-global online reconstruction system, which consolidates the 2D inconsistency and obtains robust 3D panoptic map. More qualitative 3D panoptic segmentation results are provided in our supplementary material.

**Open Vocabulary Query.** We show the qualitative open vocabulary query results of OnlineAnySeg [41] and our approach in Fig. 4. The query results of different instances are highlighted with different colors. While OnlineAnySeg can handle simple queries (e.g., “television”), it fails on some fine-grained and multi-instance queries (e.g., “pillow”, “toilet paper”, “bag”) due to inaccurate 3D instance segmenta-

tion and language feature fusion. In contrast, our clustering-based approach can obtain accurate instance-level information for objects with the same semantics. Benefiting from our local-to-global 3D instance modeling approach and fine-grained language feature fusion based on the spatial feature grid, our method can obtain more complete 3D instance information (“bag”) and distinguish different instances with the same semantics (“pillow”) in the scene.

**Runtime Analysis.** We evaluate the runtime performance of OnlinePG on a desktop computer equipped with an AMD Ryzen 9 7950X CPU and an NVIDIA RTX 4090 GPU. For Scene0645 in the ScanNetV2 dataset, our method takes an average of 410 ms to perform rendering optimization for 5 keyframes with 20 iterations, 350 ms for clustering the 12 keyframes in the sliding window, and 1400 ms for local-to-global matching and fusion (including spatial attribute updates). Since clustering and fusion process multiple keyframes per sliding window movement (frequency much lower than framerate), our system achieves 18 FPS on simple scenes and 10 FPS on complex scenes (excluding VLM computation for 2D masks and features). More detailed runtime analyses are provided in our Supp.

### 4.3. Ablation Studies

**Effects of Multiple Segments Clustering Cues.** To obtain robust and consistent 3D Gaussian instances from sliding windows, we utilized various 3D cues ( $\mathcal{O}_{ij}$ ,  $\mathcal{X}_{ij}$ ,  $\mathcal{V}_{ij}$ ) for graph clustering. On the left of Fig. 5, we show the clustering graph construction time and performance of using different cues during segment clustering to obtain consistent 3D instances. As shown in the figure, the horizontal axis represents the average time for clustering operation when using different cues, and the vertical axis represents the 3D panoptic segmentation performance,  $(\text{PRQ (T)} + \text{PRQ (S)}) / 2$ . Compared to single-cue clustering, multi-cue clustering achieves 8 to 18 PRQ improvement with only  $\sim 40$

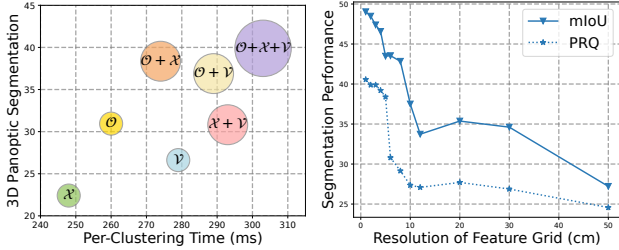


Figure 5. Left: ablation studies of using different segments clustering cues for local map construction. Right: ablation studies of using different feature grid resolutions. The results are evaluated on ScanNetV2 dataset.

ms additional latency, demonstrating a favorable accuracy-efficiency trade-off.

Table 2. Ablation studies of different matching strategies for global map fusion on ScanNetV2 dataset.

Settings	PRQ (T)	PRQ (S)
#1 NN Match	24.67	22.98
#2 Only Forward Match $\mathcal{M}_{l \rightarrow g}$	35.83	38.40
#3 Only Backward Match $\mathcal{M}_{g \rightarrow l}$	33.71	42.72
#4 Ours Full Bidirectional Match	37.97	41.81

**Effects of Bidirectional Bipartite Matching.** In Tab. 2, we show the performance of different matching strategies for fusing local map from the sliding window into global map. #1 represents using the basic nearest neighbor matching algorithm based on the forward matching matrix  $\mathcal{M}_{l \rightarrow g}$ , which obtains the matching relationship between instances in the local map and global map. Comparing #1 with others shows that using bidirectional bipartite graph matching can effectively improve accuracy for local-to-global 3D Gaussian instance fusion, with 13.3 and 18.8 improvements for PRQ (T) and PRQ (S) metrics, respectively. Comparing #2, #3 with #4, we can know that matching results obtained using bidirectional matching are more robust and accurate than those obtained using unidirectional matching. Furthermore, backward verification particularly benefits *Stuff*-level performance by improving the fusion of newly explored background regions, about 4.3 improvements over forward match for PRQ (S) metric.

Table 3. Ablation studies of our system components. The results are evaluated on ScanNetV2 dataset.

Settings	mIoU	PRQ (T)	PRQ (S)
#1 w/o. Segment Clustering	48.48	32.25	30.68
#2 w/o. Feature Grid $\mathcal{F}$	30.40	26.71	24.92
#3 Ours Full	48.48	37.97	41.81

**Effects of System Components.** In Tab. 3, we analyze the effectiveness of our segment clustering and feature grid  $\mathcal{F}$

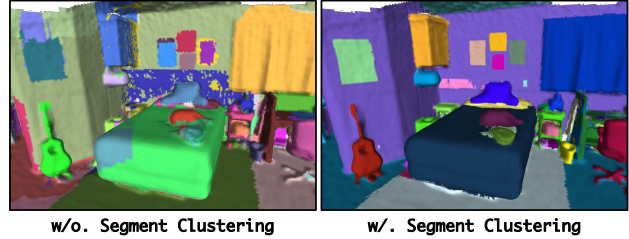


Figure 6. Qualitative comparison of using segment clustering.

inside the spatial attribute. 1) *About Segment Clustering*: #1 indicates that we directly fuse keyframe segments into the global map without clustering. Comparing #1 and #3, we can see that directly fusing noisy segments leads to incorrect segmentation of 3D instances, leading to poor panoptic understanding, especially for large *Stuff* regions. Besides, the qualitative 3D instance results of using segment clustering from Scene0000 are shown in Fig. 6. Without performing segment clustering over the local sliding window  $\mathcal{W}$ , 3D instances in the global map will contain a lot of noise. 2) *About Feature Grid*: #2 indicates we maintain a coarse language feature for each 3D instance without using feature grid  $\mathcal{F}$ . Comparing #2 and #3, we can know that our spatial attribute module can improve the open-vocabulary scene understanding performance of our system. Besides, we investigate the performance of the spatial resolution used for feature grids  $\mathcal{F}$ . The results on the ScanNetV2 dataset are shown in the right of Fig. 5, which show that spatial resolution significantly impacts performance: resolutions coarser than 5 cm cause rapid performance degradation and convergence to a lower bound.

## 5. Conclusion

We present OnlinePG, a novel and effective system for online open-vocabulary panoptic mapping using 3D Gaussian Splatting. Our approach employs a local-to-global paradigm with sliding windows to achieve efficient online reconstruction and perception. Key contributions include: (1) a multi-cue segment clustering algorithm that fuses noisy 2D priors into consistent 3D instances, (2) explicit spatial attribute grids for semantic feature storage, and (3) bidirectional bipartite matching for robust local-to-global fusion. Extensive experiments demonstrate that OnlinePG outperforms existing online methods for open-vocabulary 3D panoptic scene understanding.

**Limitations:** (1) Our method currently cannot reconstruct dynamic objects. (2) Like previous methods [41, 42, 58], we require depth and pose inputs. Our future work will explore feed-forward approaches [20, 46, 47] that eliminate these requirements for fully pose-free and depth-free open-vocabulary reconstruction.

**Acknowledgment:** This work was partially supported by NSF of China (No. 62425209).

## References

- [1] Mathilde Caron, Hugo Touvron, Ishan Misra, Hervé Jégou, Julien Mairal, Piotr Bojanowski, and Armand Joulin. Emerging properties in self-supervised vision transformers. In *IEEE/CVF International Conference on Computer Vision*, pages 9650–9660, 2021. 1, 2
- [2] Rohan Chacko, Nicolai Häni, Eldar Khaliullin, Lin Sun, and Douglas Lee. Lifting by gaussians: A simple, fast and flexible method for 3d instance segmentation. In *IEEE/CVF Winter Conference on Applications of Computer Vision*, pages 3497–3507, 2025. 2
- [3] Bowen Cheng, Maxwell D Collins, Yukun Zhu, Ting Liu, Thomas S Huang, Hartwig Adam, and Liang-Chieh Chen. Panoptic-DeepLab: A simple, strong, and fast baseline for bottom-up panoptic segmentation. In *IEEE/CVF Conference on Computer Vision and Pattern Recognition*, pages 12475–12485, 2020. 2
- [4] Bowen Cheng, Ishan Misra, Alexander G. Schwing, Alexander Kirillov, and Rohit Girdhar. Masked-attention mask transformer for universal image segmentation. In *IEEE/CVF Conference on Computer Vision and Pattern Recognition*, 2022. 2
- [5] Angela Dai, Angel X. Chang, Manolis Savva, Maciej Halber, Thomas Funkhouser, and Matthias Nießner. ScanNet: Richly-annotated 3D reconstructions of indoor scenes. In *IEEE/CVF Conference on Computer Vision and Pattern Recognition*, pages 2432–2443, 2017. 2, 5, 6, 7, 1, 3
- [6] Yitong Dong, Qi Zhang, Minchao Jiang, Zhiqiang Wu, Qingnan Fan, Ying Feng, Huaqi Zhang, Hujun Bao, and Guofeng Zhang. One-shot refiner: Boosting feed-forward novel view synthesis via one-step diffusion. *arXiv preprint arXiv:2601.14161*, 2026. 1
- [7] Xiao Fu, Shangzhan Zhang, Tianrun Chen, Yichong Lu, Lanyun Zhu, Xiaowei Zhou, Andreas Geiger, and Yiyi Liao. Panoptic NeRF: 3D-to-2D label transfer for panoptic urban scene segmentation. In *International Conference on 3D Vision*, pages 1–11, 2022. 2
- [8] Jun Guo, Xiaojian Ma, Yue Fan, Huaping Liu, and Qing Li. Semantic gaussians: Open-vocabulary scene understanding with 3d gaussian splatting, 2024. 2
- [9] Chenguang Huang, Oier Mees, Andy Zeng, and Wolfram Burgard. Visual language maps for robot navigation. In *IEEE International Conference on Robotics and Automation*, 2023. 1, 2
- [10] Cijo Jose, Théo Moutakanni, Dahyun Kang, Federico Baldassarre, Timothée Darcet, Hu Xu, Daniel Li, Marc Szafraniec, Michaël Ramamonjisoa, Maxime Oquab, Oriane Siméoni, Huy V. Vo, Patrick Labatut, and Piotr Bojanowski. Dinov2 meets text: A unified framework for image- and pixel-level vision-language alignment, 2024. 1
- [11] Bernhard Kerbl, Georgios Kopanas, Thomas Leimkühler, and George Drettakis. 3d gaussian splatting for real-time radiance field rendering. *ACM Transactions on Graphics*, 42(4), 2023. 1, 2, 3
- [12] Justin Kerr, Chung Min Kim, Ken Goldberg, Angjoo Kanazawa, and Matthew Tancik. LERF: language embedded radiance fields. In *IEEE/CVF International Conference on Computer Vision*, pages 19672–19682, 2023. 2
- [13] Alexander Kirillov, Kaiming He, Ross Girshick, Carsten Rother, and Piotr Dollár. Panoptic segmentation. In *IEEE/CVF Conference on Computer Vision and Pattern Recognition*, pages 9404–9413, 2019. 2
- [14] Alexander Kirillov, Eric Mintun, Nikhila Ravi, Hanzi Mao, Chloe Rolland, Laura Gustafson, Tete Xiao, Spencer Whitehead, Alexander C Berg, Wan-Yen Lo, et al. Segment anything. In *IEEE/CVF International Conference on Computer Vision*, pages 4015–4026, 2023. 2
- [15] Harold W Kuhn. The hungarian method for the assignment problem. *Naval research logistics quarterly*, 2(1-2):83–97, 1955. 5
- [16] Abhijit Kundu, Kyle Genova, Xiaoqi Yin, Alireza Fathi, Caroline Pantofaru, Leonidas J Guibas, Andrea Tagliasacchi, Frank Dellaert, and Thomas Funkhouser. Panoptic neural fields: A semantic object-aware neural scene representation. In *IEEE/CVF Conference on Computer Vision and Pattern Recognition*, pages 12871–12881, 2022. 1, 2
- [17] Boyi Li, Kilian Q Weinberger, Serge Belongie, Vladlen Koltun, and Rene Ranftl. Language-driven semantic segmentation. In *International Conference on Learning Representations*, 2022. 1, 2, 3, 5
- [18] Hai Li, Xingrui Yang, Hongjia Zhai, Yuqian Liu, Hujun Bao, and Guofeng Zhang. Vox-Surf: Voxel-based implicit surface representation. *IEEE Transactions on Visualization and Computer Graphics*, 30(3):1743–1755, 2022. 2
- [19] Haijie Li, Yanmin Wu, Jiarui Meng, Qiankun Gao, Zhiyao Zhang, Ronggang Wang, and Jian Zhang. InstanceGaussian: Appearance-semantic joint gaussian representation for 3d instance-level perception. In *IEEE/CVF Conference on Computer Vision and Pattern Recognition*, 2025. 1, 2, 3, 5, 6
- [20] Yuzheng Liu, Siyan Dong, Shuzhe Wang, Yingda Yin, Yanchao Yang, Qingnan Fan, and Baoquan Chen. Slam3r: Real-time dense scene reconstruction from monocular rgb videos. In *IEEE/CVF Conference on Computer Vision and Pattern Recognition*, pages 16651–16662, 2025. 8
- [21] Qi Lu, Jason Kuen, Shen Tiancheng, Gu Jiuxiang, Guo Weidong, Jia Jiaya, Lin Zhe, and Yang Ming-Hsuan. High-quality entity segmentation. In *IEEE/CVF International Conference on Computer Vision*, 2023. 2, 3, 5, 1
- [22] Tomas Berriel Martins, Martin R. Oswald, and Javier Civera. Open-vocabulary online semantic mapping for slam. *IEEE Robotics and Automation Letters*, 2025. 1, 2
- [23] Hidenobu Matsuki, Riku Murai, Paul HJ Kelly, and Andrew J Davison. Gaussian splatting slam. In *IEEE/CVF Conference on Computer Vision and Pattern Recognition*, pages 18039–18048, 2024. 1, 3
- [24] Nelson Max. Optical models for direct volume rendering. *IEEE Transactions on Visualization and Computer Graphics*, 1(2):99–108, 1995. 3
- [25] John McCormac, Ankur Handa, Andrew Davison, and Stefan Leutenegger. Semanticfusion: Dense 3d semantic mapping with convolutional neural networks. In *IEEE International Conference on Robotics and Automation*, pages 4628–4635, 2017. 2, 3, 5

- [26] Ben Mildenhall, Pratul P. Srinivasan, Matthew Tancik, Jonathan T. Barron, Ravi Ramamoorthi, and Ren Ng. Nerf: Representing scenes as neural radiance fields for view synthesis. In *European Conference on Computer Vision*, 2020. 1, 2
- [27] Arsalan Mousavian, Clemens Eppner, and Dieter Fox. 6-dof graspnet: Variational grasp generation for object manipulation. In *IEEE/CVF International Conference on Computer Vision*, pages 2901–2910, 2019. 1, 2
- [28] Gaku Narita, Takashi Seno, Tomoya Ishikawa, and Yohsuke Kaji. Panopticfusion: Online volumetric semantic mapping at the level of stuff and things. In *IEEE/RSJ International Conference on Intelligent Robots and Systems*, pages 4205–4212, 2019. 1, 2, 3, 5
- [29] Maxime Oquab, Timothée Darcet, Theo Moutakanni, Huy V. Vo, Marc Szafraniec, Vasil Khalidov, Pierre Fernandez, Daniel Haziza, Francisco Massa, Alaaeldin El-Nouby, Russell Howes, Po-Yao Huang, Hu Xu, Vasu Sharma, Shang-Wen Li, Wojciech Galuba, Mike Rabbat, Mido Assran, Nicolas Ballas, Gabriel Synnaeve, Ishan Misra, Herve Jegou, Julien Mairal, Patrick Labatut, Armand Joulin, and Piotr Bojanowski. Dinov2: Learning robust visual features without supervision, 2023. 1
- [30] Xiaokun Pan, Zhenzhe Li, Zhichao Ye, Hongjia Zhai, and Guofeng Zhang. Egg-fusion: Efficient 3d reconstruction with geometry-aware gaussian surfel on the fly. In *Proceedings of the SIGGRAPH Asia 2025 Conference Papers*, pages 1–12, 2025. 2
- [31] Songyou Peng, Kyle Genova, Chiyu "Max" Jiang, Andrea Tagliasacchi, Marc Pollefeys, and Thomas Funkhouser. Openscene: 3d scene understanding with open vocabularies. In *IEEE/CVF Conference on Computer Vision and Pattern Recognition*, 2023. 1, 2, 5, 6, 7
- [32] Lorenzo Porzi, Samuel Rota Bulò, Aleksander Colovic, and Peter Kotschieder. Seamless scene segmentation. In *IEEE/CVF conference on computer vision and pattern recognition*, pages 8277–8286, 2019. 2
- [33] Minghan Qin, Wanhua Li, Jiawei Zhou, Haoqian Wang, and Hanspeter Pfister. Langsplat: 3d language gaussian splatting. In *IEEE/CVF Conference on Computer Vision and Pattern Recognition*, pages 20051–20060, 2024. 1, 5, 6, 7
- [34] Alec Radford, Jong Wook Kim, Chris Hallacy, Aditya Ramesh, Gabriel Goh, Sandhini Agarwal, Girish Sastry, Amanda Askell, Pamela Mishkin, Jack Clark, et al. Learning transferable visual models from natural language supervision. In *International Conference on Machine Learning*, pages 8748–8763, 2021. 1, 2, 5
- [35] Nikhila Ravi, Valentin Gabeur, Yuan-Ting Hu, Ronghang Hu, Chaitanya Ryali, Tengyu Ma, Haitham Khedr, Roman Rädle, Chloe Rolland, Laura Gustafson, Eric Mintun, Jungmin Pan, Kalyan Vasudev Alwala, Nicolas Carion, Chao-Yuan Wu, Ross Girshick, Piotr Dollár, and Christoph Feichtenhofer. Sam 2: Segment anything in images and videos. *arXiv preprint arXiv:2408.00714*, 2024. 1
- [36] Erik Sandström, Yue Li, Luc Van Gool, and Martin R. Oswald. Point-slam: Dense neural point cloud-based slam. In *IEEE/CVF International Conference on Computer Vision*, 2023. 2
- [37] Jonas Schult, Francis Engelmann, Alexander Hermans, Or Litany, Siyu Tang, and Bastian Leibe. Mask3D: Mask Transformer for 3D Semantic Instance Segmentation. In *International Conference on Robotics and Automation*, 2023. 2
- [38] Jin-Chuan Shi, Miao Wang, Hao-Bin Duan, and Shao-Hua Guan. Language embedded 3d gaussians for open-vocabulary scene understanding. In *IEEE/CVF Conference on Computer Vision and Pattern Recognition*, pages 5333–5343, 2024. 1, 2
- [39] Yawar Siddiqui, Lorenzo Porzi, Samuel Rota Bulò, Norman Müller, Matthias Nießner, Angela Dai, and Peter Kotschieder. Panoptic lifting for 3d scene understanding with neural fields. In *IEEE/CVF Conference on Computer Vision and Pattern Recognition*, pages 9043–9052, 2023. 2
- [40] Julian Straub, Thomas Whelan, Lingni Ma, Yufan Chen, Erik Wijmans, Simon Green, Jakob J. Engel, Raul Mur-Artal, Carl Ren, Shobhit Verma, Anton Clarkson, Mingfei Yan, Brian Budge, Yajie Yan, Xiaqing Pan, June Yon, Yuyang Zou, Kimberly Leon, Nigel Carter, Jesus Briales, Tyler Gillingham, Elias Mueggler, Luis Pesqueira, Manolis Savva, Dhruv Batra, Hauke M. Strasdat, Renzo De Nardi, Michael Goesele, Steven Lovegrove, and Richard Newcombe. The Replica dataset: A digital replica of indoor spaces. *arXiv preprint arXiv:1906.05797*, 2019. 2, 5, 6, 1, 3
- [41] Yijie Tang, Jiazhao Zhang, Yuqing Lan, Yulan Guo, Dezun Dong, Chenyang Zhu, and Kai Xu. Onlineanyscg: Online zero-shot 3d segmentation by visual foundation model guided 2d mask merging. In *IEEE/CVF Conference on Computer Vision and Pattern Recognition*, pages 3676–3685, 2025. 2, 5, 6, 7, 8, 1, 3
- [42] Muer Tie, Julong Wei, Ke Wu, Zhengjun Wang, Shanshuai Yuan, Kaizhao Zhang, Jie Jia, Jieru Zhao, Zhongxue Gan, and Wenchao Ding. O2v-mapping: Online open-vocabulary mapping with neural implicit representation. In *European Conference on Computer Vision*, pages 318–333, 2024. 2, 5, 6, 8, 3
- [43] Vadim Tschernezki, Iro Laina, Diane Larlus, and Andrea Vedaldi. Neural feature fusion fields: 3d distillation of self-supervised 2d image representations. In *International Conference on 3D Vision*, pages 443–453, 2022. 2
- [44] Thang Vu, Kookhoi Kim, Tung M Luu, Thanh Nguyen, and Chang D Yoo. Softgroup for 3d instance segmentation on point clouds. In *IEEE/CVF Conference on Computer Vision and Pattern Recognition*, pages 2708–2717, 2022. 2, 6, 7
- [45] Hengyi Wang, Jingwen Wang, and Lourdes Agapito. Co-SLAM: joint coordinate and sparse parametric encodings for neural real-time slam. In *IEEE/CVF Conference on Computer Vision and Pattern Recognition*, 2023. 2
- [46] Jianyuan Wang, Minghao Chen, Nikita Karaev, Andrea Vedaldi, Christian Rupprecht, and David Novotny. Vggt: Visual geometry grounded transformer. In *IEEE/CVF Conference on Computer Vision and Pattern Recognition*, pages 5294–5306, 2025. 8
- [47] Shuzhe Wang, Vincent Leroy, Johann Cabon, Boris Chidlovskii, and Jerome Revaud. Dust3r: Geometric 3d vision made easy. In *IEEE/CVF Conference on Computer Vision and Pattern Recognition*, pages 20697–20709, 2024. 8

- [48] Zhigang Wang, Yifei Su, Chenhui Li, Dong Wang, Yan Huang, Xuelong Li, and Bin Zhao. Open-vocabulary octree-graph for 3d scene understanding. In *IEEE/CVF International Conference on Computer Vision*, pages 7037–7047, 2025. 1
- [49] Dong Wu, Zike Yan, and Hongbin Zha. Panorecon: Real-time panoptic 3d reconstruction from monocular video. In *IEEE/CVF Conference on Computer Vision and Pattern Recognition*, pages 21507–21518, 2024. 1
- [50] Yanmin Wu, Jiarui Meng, Haijie Li, Chenming Wu, Yahao Shi, Xinhua Cheng, Chen Zhao, Haocheng Feng, Errui Ding, Jingdong Wang, and Jian Zhang. Opengaussian: Towards point-level 3d gaussian-based open vocabulary understanding. In *Advances in Neural Information Processing Systems*, 2024. 1, 2, 3, 5, 6, 7
- [51] Xiuwei Xu, Huangxing Chen, Linqing Zhao, Ziwei Wang, Jie Zhou, and Jiwen Lu. Embodiedsam: Online segment any 3d thing in real time. *arXiv preprint arXiv:2408.11811*, 2024. 2
- [52] Kashu Yamazaki, Taisei Hanyu, Khoa Vo, Thang Pham, Minh Tran, Gianfranco Doretto, Anh Nguyen, and Ngan Le. Open-fusion: Real-time open-vocabulary 3d mapping and queryable scene representation. In *IEEE International Conference on Robotics and Automation*, pages 9411–9417, 2024. 2
- [53] Mi Yan, Jiazhao Zhang, Yan Zhu, and He Wang. Maskclustering: View consensus based mask graph clustering for open-vocabulary 3d instance segmentation. In *IEEE/CVF Conference on Computer Vision and Pattern Recognition*, pages 28274–28284, 2024. 4
- [54] Xingrui Yang, Hai Li, Hongjia Zhai, Yuhang Ming, Yuqian Liu, and Guofeng Zhang. Vox-Fusion: Dense tracking and mapping with voxel-based neural implicit representation. In *IEEE International Symposium on Mixed and Augmented Reality*, pages 499–507, 2022. 2
- [55] Mingqiao Ye, Martin Danelljan, Fisher Yu, and Lei Ke. Gaussian grouping: Segment and edit anything in 3d scenes. In *European Conference on Computer Vision*, 2024. 2, 3
- [56] Hongjia Zhai, Gan Huang, Qirui Hu, Guanglin Li, Hujun Bao, and Guofeng Zhang. NIS-SLAM: Neural implicit semantic RGB-D SLAM for 3D consistent scene understanding. *IEEE Transactions on Visualization and Computer Graphics*, 30(11):7129–7139, 2024. 2
- [57] Hongjia Zhai, Hai Li, Xingrui Yang, Gan Huang, Yuhang Ming, Hujun Bao, and Guofeng Zhang. Vox-fusion++: Voxel-based neural implicit dense tracking and mapping with multi-maps. *arXiv preprint arXiv:2403.12536*, 2024. 2
- [58] Hongjia Zhai, Hai Li, Zhenzhe Li, Xiaokun Pan, Yijia He, and Guofeng Zhang. Panogs: Gaussian-based panoptic segmentation for 3d open vocabulary scene understanding. In *IEEE/CVF Conference on Computer Vision and Pattern Recognition*, pages 14114–14124, 2025. 1, 2, 5, 6, 7, 8
- [59] Hongjia Zhai, Xiyu Zhang, Boming Zhao, Hai Li, Yijia He, Zhaopeng Cui, Hujun Bao, and Guofeng Zhang. Splat-Loc: 3d gaussian splatting-based visual localization for augmented reality. *IEEE Transactions on Visualization and Computer Graphics*, 31(5):3591–3601, 2025. 2
- [60] Hongjia Zhai, Boming Zhao, Hai Li, Xiaokun Pan, Yijia He, Zhaopeng Cui, Hujun Bao, and Guofeng Zhang. Neuraloc: Visual localization in neural implicit map with dual complementary features. In *IEEE International Conference on Robotics and Automation*, pages 11706–11713, 2025. 2
- [61] Jiazhao Zhang, Liu Dai, Fanpeng Meng, Qingnan Fan, Xuelin Chen, Kai Xu, and He Wang. 3d-aware object goal navigation via simultaneous exploration and identification. In *IEEE/CVF Conference on Computer Vision and Pattern Recognition*, pages 6672–6682, 2023. 1, 2
- [62] Xiyu Zhang, Chong Bao, YiPeng Chen, Hongjia Zhai, Yitong Dong, Hujun Bao, Zhaopeng Cui, and Guofeng Zhang. AtlasGS: Atlanta-world guided surface reconstruction with implicit structured gaussians. In *Annual Conference on Neural Information Processing Systems*, 2025. 2
- [63] Shijie Zhou, Haoran Chang, Sicheng Jiang, Zhiwen Fan, Zehao Zhu, Dejie Xu, Pradyumna Chari, Suyu You, Zhanqiang Wang, and Achuta Kadambi. Feature 3dgs: Supercharging 3d gaussian splatting to enable distilled feature fields. In *IEEE/CVF Conference on Computer Vision and Pattern Recognition*, pages 21676–21685, 2024. 2
- [64] Runsong Zhu, Shi Qiu, Qianyi Wu, Ka-Hei Hui, Pheng-Ann Heng, and Chi-Wing Fu. Pcf-lift: Panoptic lifting by probabilistic contrastive fusion. In *European Conference on Computer Vision*, pages 92–108. Springer, 2025. 2
- [65] Siting Zhu, Ziyun Lu, Guangming Wang, Chenguang Huang, Yongbo Chen, I-Ming Chen, Wolfram Burgard, and Hesheng Wang. OgsScene3d: Incremental open-vocabulary 3d gaussian scene graph mapping for scene understanding. *arXiv preprint arXiv:2603.16301*, 2026. 2
- [66] Xingxing Zuo, Pouya Samangouei, Yunwen Zhou, Yan Di, and Mingyang Li. FMGS: Foundation model embedded 3D gaussian splatting for holistic 3D scene understanding. *International Journal of Computer Vision*, pages 1–17, 2024. 2

# OnlinePG: Online Open-Vocabulary Panoptic Mapping with 3D Gaussian Splatting

## Supplementary Material

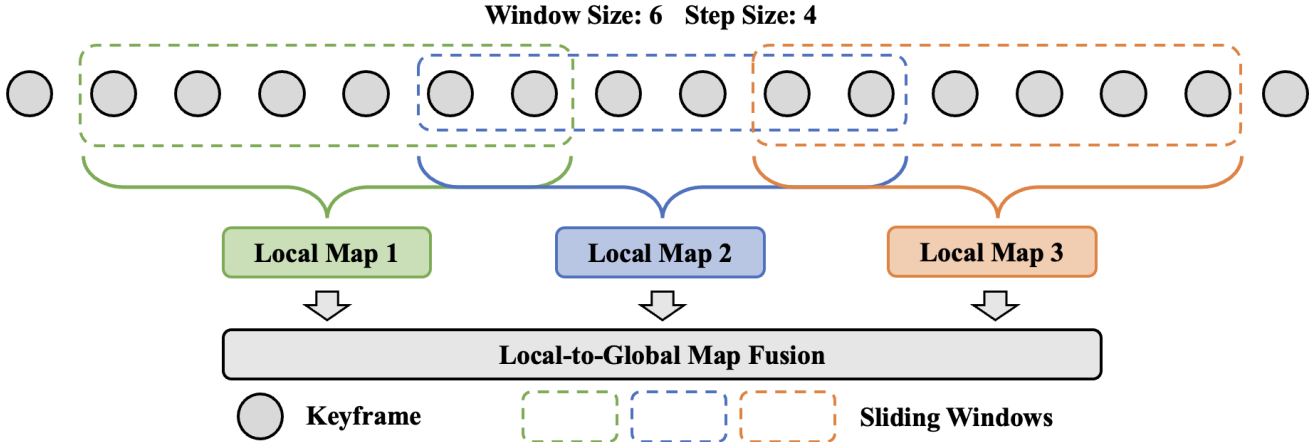


Figure 7. **Illustration of Sliding Window.** For a sliding window with a size of 6 and a step size of 4, we perform segment clustering every 4 keyframes and merge the local map into the global map. As shown in the figure, this reduces the reading and updating of the global map, enabling efficient reconstruction.

In this supplementary document, we first provide more implementation details in Sec. 6. Next, we supply more visualization results of our methods in Sec. 7.

## 6. Implementation Details

**Dataset Setting** For ScanNetV2 [5], we use the following 10 scenes: *scene0000*, *scene0062*, *scene0070*, *scene0097*, *scene0140*, *scene0200*, *scene0347*, *scene0400*, *scene0590*, and *scene0645*. All selected scenes are evaluated on the 00 trajectory. For the evaluation of 3D semantic and panoptic segmentation, we use the 19 classes: *wall*, *floor*, *cabinet*, *bed*, *sofa*, *table*, *door*, *window*, *bookshelf*, *picture*, *counter*, *desk*, *curtain*, *refrigerator*, *shower curtain*, *toilet*, *sink*, and *bathtub*. For Replica dataset [40], the commonly-used 8 scenes  $\{room0-2, office0-4\}$  are used for evaluation, and two additional labels, *other furniture* and *ceiling*, are used for evaluation.

**Details of Our OnlinePG** Following [31, 50, 58], we adopt CLIP [34] and LSeg [17] as text and image visual-language feature extractors, with feature dimension  $D_f = 512$ . We use EntitySeg [21] to extract 2D instance segmentation for each keyframe. We sample a keyframe every 20 frames and maintain a sliding window of size 12. Segment clustering and local-to-global map fusion are performed every 7 keyframes. The illustration of sliding window design is shown in Fig. 7. For an online image stream, we maintain a fixed-size window and move it in fixed steps. Each time the sliding window moves, it builds a local map for

all keyframes in the window and merges it into the global map based on bidirectional matching. The resolutions of the Replica [40] and ScanNetV2 [5] datasets that we used are  $640 \times 360$  and  $640 \times 480$ , respectively. When performing bidirectional bipartite matching between the local and global maps, we remove matches with scores below the threshold  $1/N_{ins}$  to filter out erroneous results, where  $N_{ins}$  is the number of candidate matches. For rendering optimization, the learning rates for the 3D Gaussian’s location, opacity, scale, color, and rotation are set to 0.00015, 0.05, 0.001, 0.001, 0.01, respectively.

**Runtime Analysis** Because the running speed of our method is affected by the number of masks in the 2D image and the number of instances in the 3D scene, we report the running time in 10 selected scenes from ScanNetV2. For the video stream, we select one frame every 20 frames as a keyframe and process it. As shown in Fig. 8, we show the runtime of four main parts in our system: (#1) Keyframe Preprocessing and 3D Segments Initialization, (#2) 3DGS Optimization, (#3) Segment Clustering, and (#4) Local-to-Global Map Fusion. #1 and #2 are called once every time a new keyframe is inserted. #3 and #4 are called only when the sliding window moves a fixed step size.

Besides, the FPS performance of different online methods is also shown in Tab. 4 and Tab. 5. Since OnlineAnySeg [41] needs to obtain the mask and features in advance, the FPS results reported by different methods in the table do not include the time of VLM inference.

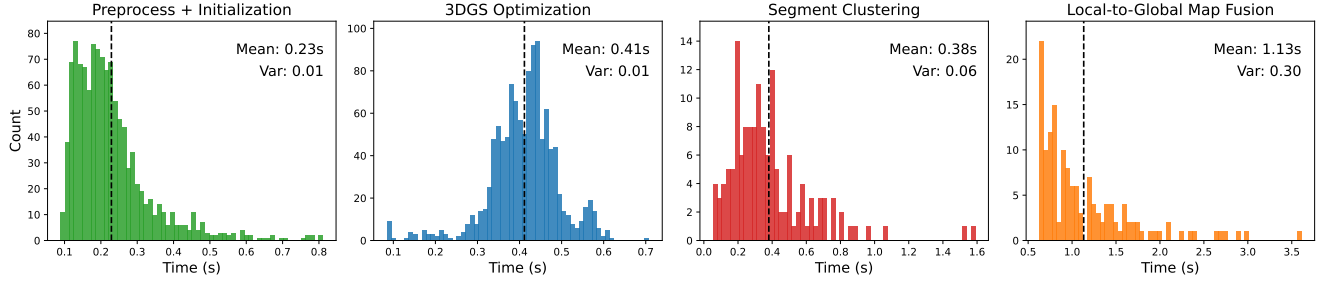


Figure 8. **Runtime Performance of OnlinePG.** We divided the system’s time consumption into four parts and statistically analyzed the distribution of the execution time of each part across ten scenarios used by ScanNet. The black dashed line represents the average time.

## 7. More Experimental Results

**Detailed Performance of Each Scene** The detailed 3D semantic and panoptic segmentation performance of our approach and different online baselines (O2V-Mapping [42] and OnlineAnySeg [41]) are shown in Tab. 4 and Tab. 5, respectively.

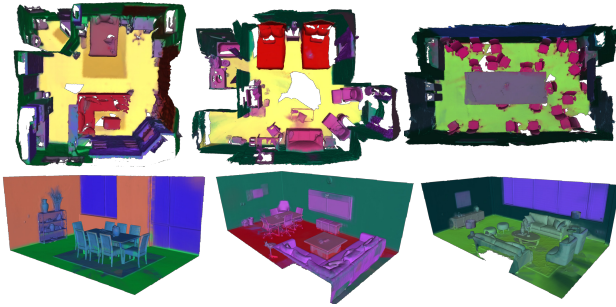


Figure 9. **Visualization Results of 3D Language Features.** For better visualization, we perform principal components analysis (PCA) on the high-dimensional language features.

**3D Language Feature** In Fig. 9, we show the visualization results of the language features reconstructed by our OnlinePG. We used principal component analysis to compress the 512-dimensional features into 3 dimensions for visualization. As can be seen from the figure, the features we obtained can distinguish finer-grained objects, such as carpet and floor, bed and sofa, *etc.* Objects with semantic similarity have similar characteristics, and visualization can show that they have similar colors.

**Rendering Results** In Fig. 10, we present rendering results from four viewpoints on the ScanNetV2 [5] and Replica [40] datasets, including RGB, depth, and language features.

**3D Instance Results** In Fig. 11, we present 3D instance segmentation results of some scene from the ScanNetV2 [5] and Replica [40] datasets. Different colors represent different 3D instances. Due to the GT mesh of the Replica dataset containing many unobserved areas in the images, this will

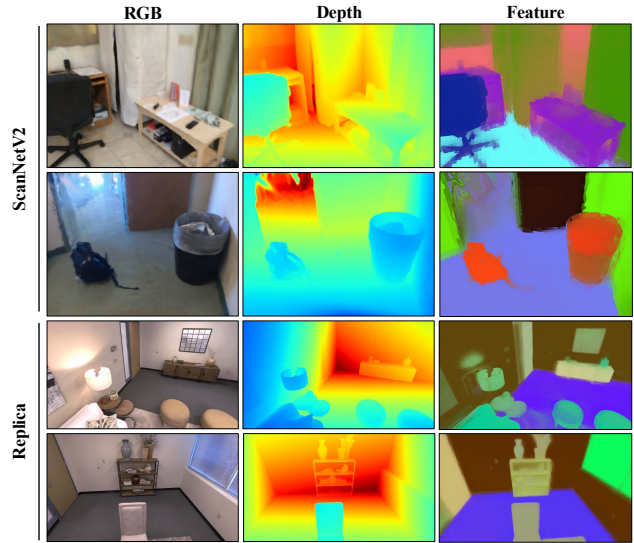


Figure 10. **Qualitative Rendering Results.** We show the rendered RGB, Depth, and language feature of different scenes.

lead to some noisy instances (on the floor and walls), which will also cause the PRQ (S) of the online method to be worse than that of the offline method.

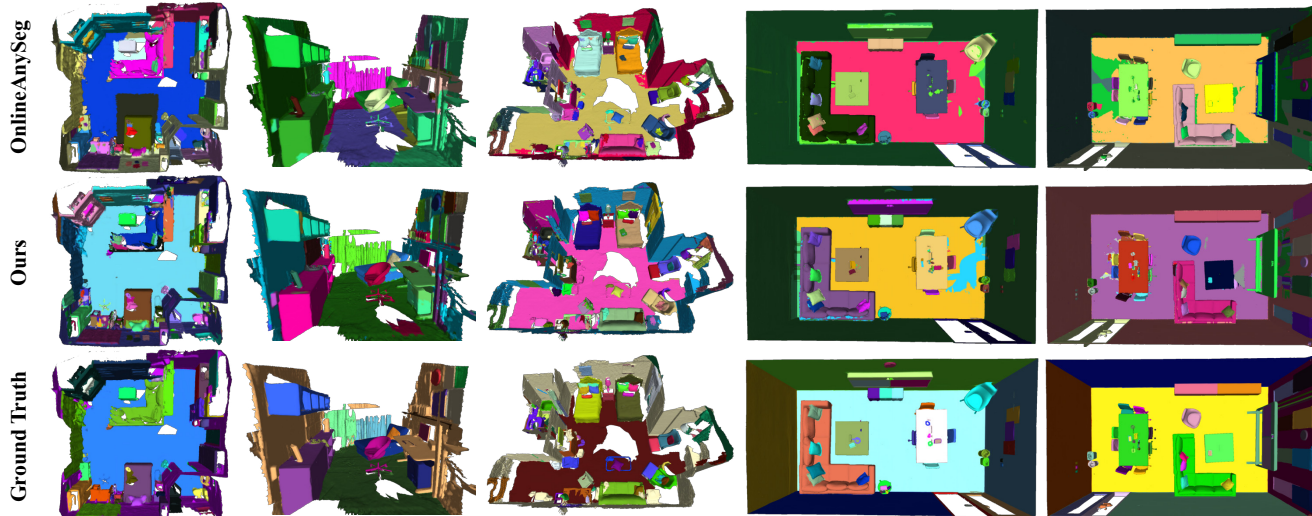


Figure 11. **Qualitative 3D Instance Segmentation Comparison.** We show the 3D instance segmentation results from several scenes from ScanNetV2 [5] and Replica [40] datasets.

Table 4. **3D Semantic and Panoptic Segmentation Results on Replica Datasets.** We demonstrate the 3D segmentation performance and FPS data of the online method in different scenes of Replica [40].

Method	Metrics	Room 0	Room 1	Room 2	Office 0	Office 1	Office 2	Office 3	Office 4
O2V-Mapping [42]	mIoU	29.25	39.58	32.53	18.78	17.54	20.75	12.59	23.24
	mAcc.	38.00	52.60	43.22	27.56	20.25	30.20	17.95	38.47
	FPS	3.08	3.05	3.08	3.05	3.10	3.13	3.18	3.28
OnlineAnySeg [41]	mIoU	46.76	45.13	51.30	37.54	25.38	32.91	25.45	48.23
	mAcc.	62.41	67.50	66.84	50.47	31.24	46.99	42.46	59.45
	PRQ (T)	30.26	51.65	26.59	45.34	22.10	24.90	16.32	27.17
	PRQ (S)	8.58	15.99	10.97	8.65	2.73	7.15	4.83	11.46
	FPS	9.90	13.06	12.91	15.40	20.94	11.65	10.81	11.45
Ours	mIoU	53.60	67.16	68.31	32.07	10.19	53.53	54.95	43.55
	mAcc.	59.34	80.17	75.86	36.28	16.07	60.06	60.86	50.96
	PRQ (T)	31.03	57.49	51.14	48.45	0.00	48.40	47.46	43.89
	PRQ (S)	11.75	17.22	12.44	7.37	4.47	17.48	9.20	18.05
	FPS	12.07	13.91	14.07	15.85	18.22	14.77	12.42	14.14

Table 5. **3D Semantic and Panoptic Segmentation Results on ScanNetV2 Datasets.** We demonstrate the 3D segmentation performance and FPS data of the online method in different scenes of ScanNetV2 [5].

Method	Metrics	0000	0062	0070	0097	0140	0200	0347	0400	0590	0645
O2V-Mapping [42]	mIoU	35.80	46.09	41.21	26.29	24.25	39.08	27.54	39.74	33.18	28.27
	mAcc.	59.92	72.72	55.59	55.73	34.15	63.91	47.12	58.33	49.85	52.22
	FPS	3.38	3.43	3.43	3.53	3.40	3.50	3.43	3.38	3.43	3.38
OnlineAnySeg [41]	mIoU	32.64	31.13	23.26	39.08	12.62	39.32	32.97	33.93	34.66	33.26
	mAcc.	50.61	60.73	31.92	69.62	31.86	52.43	54.51	56.42	55.89	58.02
	PRQ (T)	42.32	33.47	36.29	71.30	53.32	33.76	38.43	25.97	38.95	56.06
	PRQ (S)	18.53	38.20	12.89	41.70	7.94	39.09	20.35	38.26	24.50	21.32
	FPS	15.57	22.91	26.44	22.83	15.72	19.27	20.41	25.22	22.98	16.93
Ours	mIoU	39.75	75.09	46.50	52.59	48.04	47.84	52.76	39.44	37.95	44.92
	mAcc.	61.77	90.36	62.95	70.39	64.54	62.11	72.50	62.18	53.33	60.05
	PRQ (T)	20.21	35.28	49.55	58.63	51.67	46.56	42.08	0.00	33.55	42.16
	PRQ (S)	40.05	63.27	24.34	52.79	39.28	43.94	36.68	56.53	33.36	27.88
	FPS	13.33	18.83	15.68	17.57	14.23	18.48	17.86	16.89	15.26	14.08